# Depth profiles of suspended carbon and nitrogen along a North Pacific transect: Concentrations, isotopes, and ratios

Sijia Dong [1*], Xingchen Tony Wang,[2*] Adam V. Subhas [3], Frank J. Pavia,[1] Jess F. Adkins,[1] William M. Berelson[4]
[1]California Institute of Technology, Pasadena, California
[2]Boston College, Chestnut Hill, Massachusetts
[3]Woods Hole Oceanographic Institution, Woods Hole, Massachusetts
[4]University of Southern California, California, Los Angeles

## Abstract

We present concentrations of total particulate carbon (PC), carbonate (PIC), total particulate nitrogen (PN), $\delta^{13}C$ and $\delta^{15}N$ of suspended particles along a North Pacific transect. In the upper 400 m, suspended PIC to particulate organic carbon (POC) ratios generally follow published sinking PIC/POC ratios. Below 600 m, suspended PIC/POC become significantly lower than sinking PIC/POC, likely indicating PIC dissolution within the suspended load. In three out of the five stations, suspended PN $\delta^{15}N$ increase with depth from the euphotic zone to the thermocline, consistent with previous observations in many ocean regions (e.g.,BATS and HOT). However, in the other two stations where phytoplankton blooms were encountered, high suspended PN $\delta^{15}N$ (up to 12‰) were observed in the euphotic zone, which was likely caused by the export of low-$\delta^{15}N$ PN during the phytoplankton blooms. Average $C_{org} : N$ ratio of suspended particles along the transect is 5.1 ± 0.2, with the value in the subtropical gyre (5.8 ± 0.3) slightly higher than the subarctic gyre (4.6 ± 0.2).

Biological production in the euphotic zone converts dissolved carbon species into particulate organic matter, which sinks downward to the deep ocean after the death of the organisms. This process, known as the soft tissue pump, drives the uptake of atmospheric $CO_2$ into seawater by lowering the dissolved inorganic carbon (DIC) concentration of the surface ocean. Some organisms also convert dissolved inorganic carbon into solid calcium carbonate shells. Even though the production of biological $CaCO_3$ in the euphotic zone tends to increase atmospheric $CO_2$ by decreasing the alkalinity in the surface water, the ballasting of organic matter by $CaCO_3$ (Armstrong et al. 2002; Klaas and Archer 2002) can increase the sinking velocity of the particle aggregates, therefore promoting the burial and long-time storage of C at the seafloor. The dissolution of $CaCO_3$ in the water column, on the other hand, drives up alkalinity and therefore lowers $pCO_2$. As a result, understanding where and how fast organic matter and inorganic carbon decompose/dissolve in the ocean is vital in determining the ocean's capacity to store carbon and buffer anthropogenic $CO_2$ release.

Nearly all models of carbonate cycling in the ocean rely on some formulation of the export ratio of particulate inorganic carbon (PIC) to particulate organic carbon (POC)—PIC/POC (Jansen et al. 2002; Sarmiento et al. 2002; Jokulsdottir and Archer 2015). These models usually predict POC production via phosphorus uptake, and then use the PIC/POC ratio to scale to PIC. Therefore, field observations of the values and variability in PIC/POC are vital to constrain carbonate cycling and diagnose the reliability of the model results. While PIC/POC in net community production and settling particles is widely studied (Rodier and Le Borgne 1997; Berelson et al. 2007; Honjo et al. 2008), less is known for suspended PIC/POC. Suspended particles in the water column represent a wide range of inputs, including biogenic components, lithogenic and authigenic minerals, and the semi-decomposed phase of sinking particles. They carry important information of surface productivity and subsequent particle dynamics processes, including particle aggregation and disaggregation, sinking, organic matter remineralization, and PIC dissolution in the water column (Lam et al. 2018).

In addition to directly investigating C content and $\delta^{13}C$ in the suspended particles, the analysis of PN provides important constraints on the biological and chemical processes in the water column. $\delta^{15}N$ of suspended PN in the euphotic zone is influenced by the $\delta^{15}N$ of N substrates and isotopic

*Correspondence: dongsj@caltech.edu; xingchen.wang@bc.edu

fractionation during PN formation and recycling; and has been widely used to study nitrogen cycling in the upper ocean (Altabet 1988; Minagawa et al. 2001; Yamaguchi and McCarthy 2018). Another tracer for biogeochemical processes in the water column is $N^* = [NO_3^-] - 16[PO_4^{3-}] + 2.9\,\mu mol\ kg^{-1}$ (Gruber and Sarmiento 1997; Gruber 2008). The $N^*$ value is affected by denitrification and $N_2$ fixation, and has therefore been related to nitrate $\delta^{15}N$, which is affected by these same processes (Altabet et al. 1999; Minagawa et al. 2001). Spatial variations in the Redfield stoichiometry of exported particles may affect the estimates of global carbon export (Teng et al. 2014) and the coupling of the cycles of nutrients, oxygen and carbon (Devries and Deutsch 2014).

Although the $\delta^{13}C$ and $\delta^{15}N$ of suspended particles have been frequently reported for the upper ocean, such data from the deep ocean are relatively rare. In this study, we report concentrations, isotope values, and C : N ratios for suspended particles along a North Pacific transect near 150°W from the surface to ~ 5000 m. We also report $N^*$ along the transect and combine the $N^*$ concentrations with the particle measurements to investigate the production, export, and the subsequent decomposition of organic matter and calcium carbonate. The determination of concentrations and isotope values of suspended particles adds to the scarce biogeochemical database in the open ocean of the North Pacific.

## Materials and methods

### Study area

A 30-day research cruise, CDisK-IV, was conducted from Honolulu, Hawaii to Seward, Alaska (near 150°W) in August, 2017. Particle and water samples were collected at five stations along the North Pacific transect (Fig. 1a). The cruise crossed from the subtropical gyre to the subarctic gyre, passing through the transition zone, which is known for high productivity and particle export (Bograd et al. 2004; Juranek et al. 2012; Polovina et al. 2017). The subarctic gyre is relatively more nutrient-rich than the oligotrophic subtropical gyre (Conkright et al. 2002) and therefore has higher primary productivity (Kawahata 1998; Eguchi et al. 2003). The high productivity in the transition zone, and the difference between the subtropical and subarctic gyre are consistent with a Sta. 4 peak in sinking PIC and POC fluxes obtained from floating traps deployed at 100 m and 200 m (Fig. 1b; Dong et al. 2019). The Transition Zone Chlorophyll Front (TZCF) migrates seasonally between 30°N in winter and 45°N in summer (Polovina et al. 2001; Ayers and Lozier 2010), and was located at ~ 37°N during the CDisK-IV cruise based on fluorescence data and high-resolution particle size spectra collected with an Underway Vision Profiler (Dugenne, pers. comm.; Hou et al. 2019). Based on NASA satellite data, the TZCF was further to the south, at Sta. 3 (35°N, dashed line) in May 2017 (Fig. 1c). Therefore, Sta. 3 was a unique station that had a high
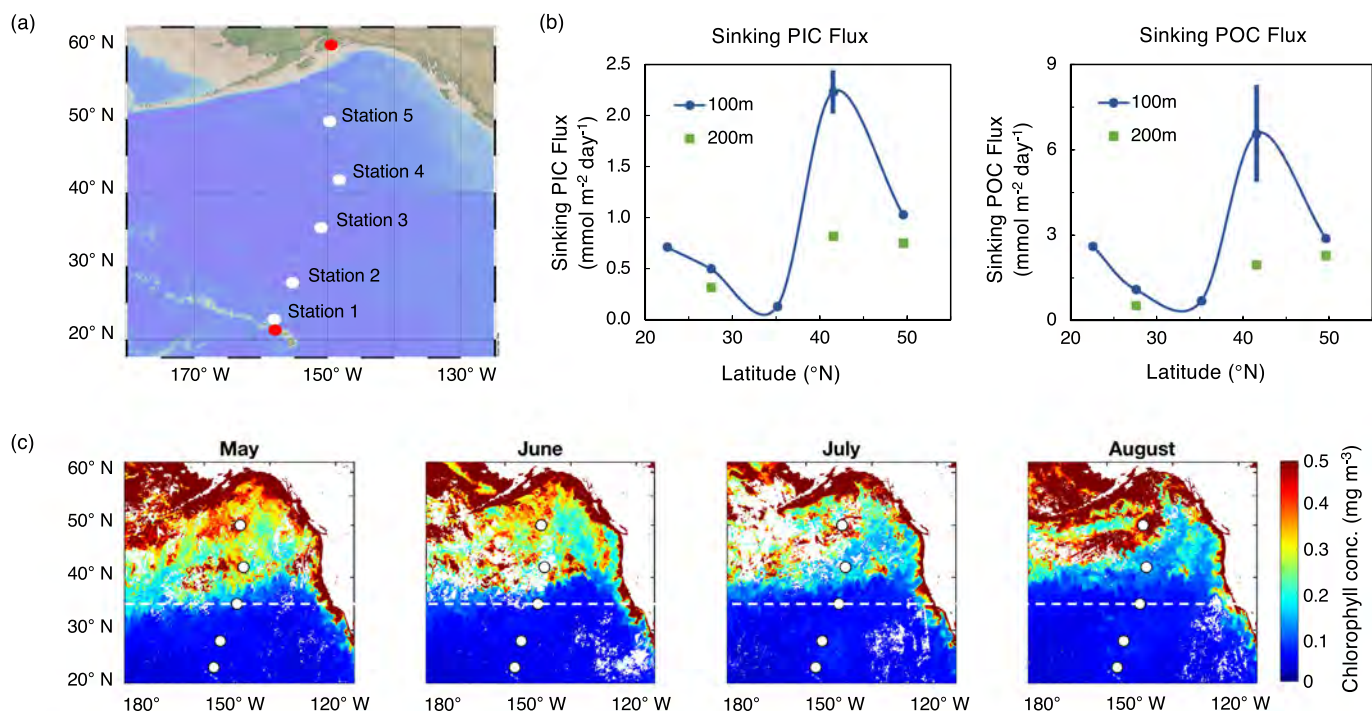


**Fig. 1.** Location and productivity of the CDisK-IV stations. **(a)** A map of the Northeast Pacific and station locations for the CDisK-IV cruise (August, 2017). **(b)** Export production of PIC and POC (sinking particles) at 100 and 200 m determined by sediment traps during CDisK-IV (Dong et al. 2019). **(c)** Surface chlorophyll concentration determined by NASA satellite data from May, 2017 to August, 2017. Dashed line indicates the latitude of Sta. 3.
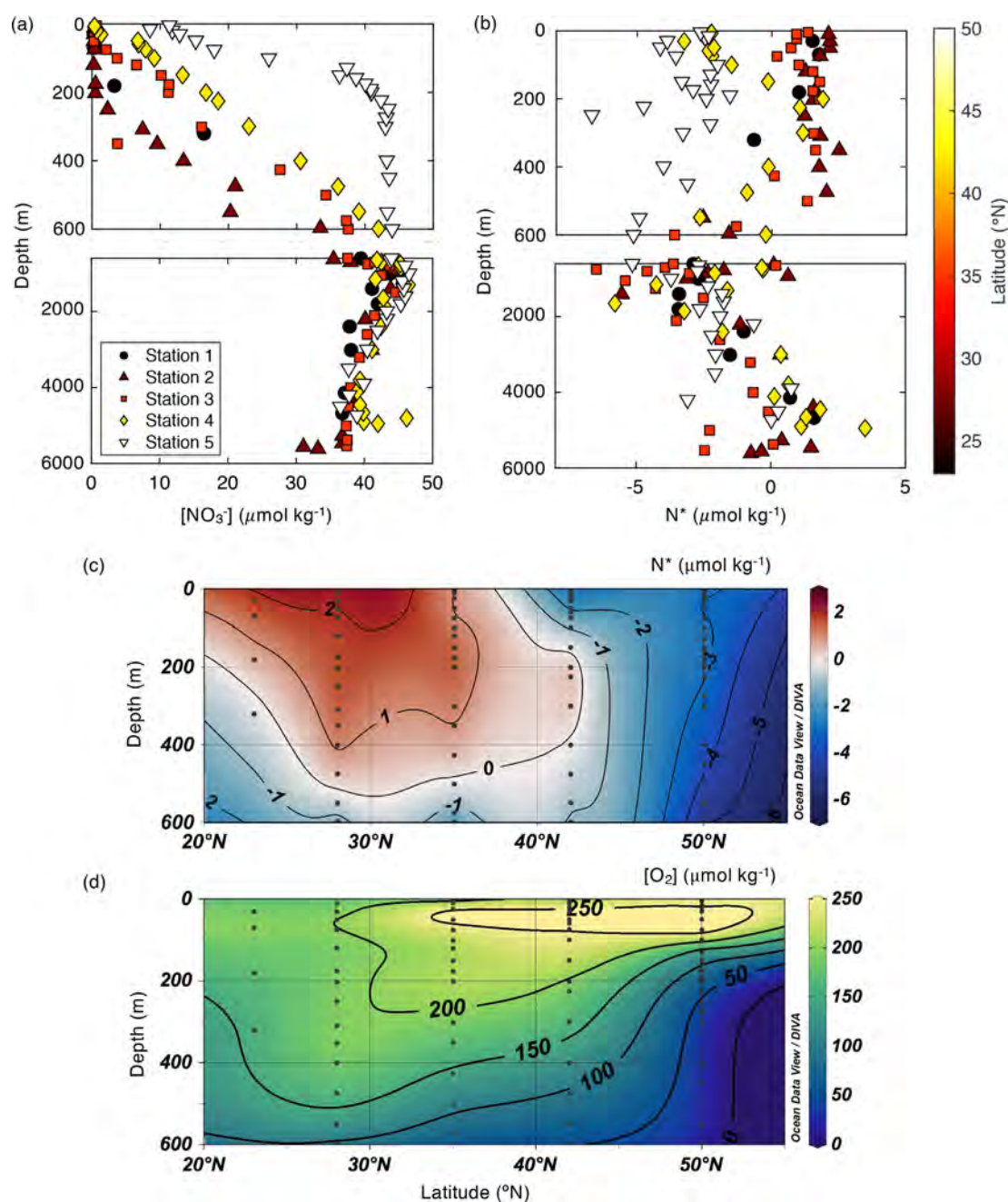
**Fig. 2.** Nutrient and $O_2$ concentration along the North Pacific transect. **(a)** Nitrate concentration vs. depth. **(b)** $N^*$ vs. depth. **(c)** Distribution of $N^*$ along the transect. **(d)** $O_2$ concentration along the transect.

productivity earlier in the year (winter and spring), possibly a productivity peak 3 months before CDisK-IV, and then low productivity during CDisK-IV; whereas Sta. 4 was likely at its productivity peak during CDisK-IV.

### Analysis of nutrients and potential density of the water column

Water samples were collected through Conductivity, Temperature, Depth (CTD) casts using the 10-L Niskin Rosette on the R/V Kilo Moana, and 50 mL samples from each depth were filtered through 0.45-$\mu$m syringe filters immediately after the CTD deployment during CDisK-IV. Nitrate and phosphate concentrations were determined using colorimetric methods at the Chesapeake Biological Laboratory, Solomons Island, University of Maryland. The potential density ($\sigma_\theta$) of the water column was calculated based on the pressure, temperature, and salinity values determined during the CTD casts, and was calculated relative to the surface (0 m).
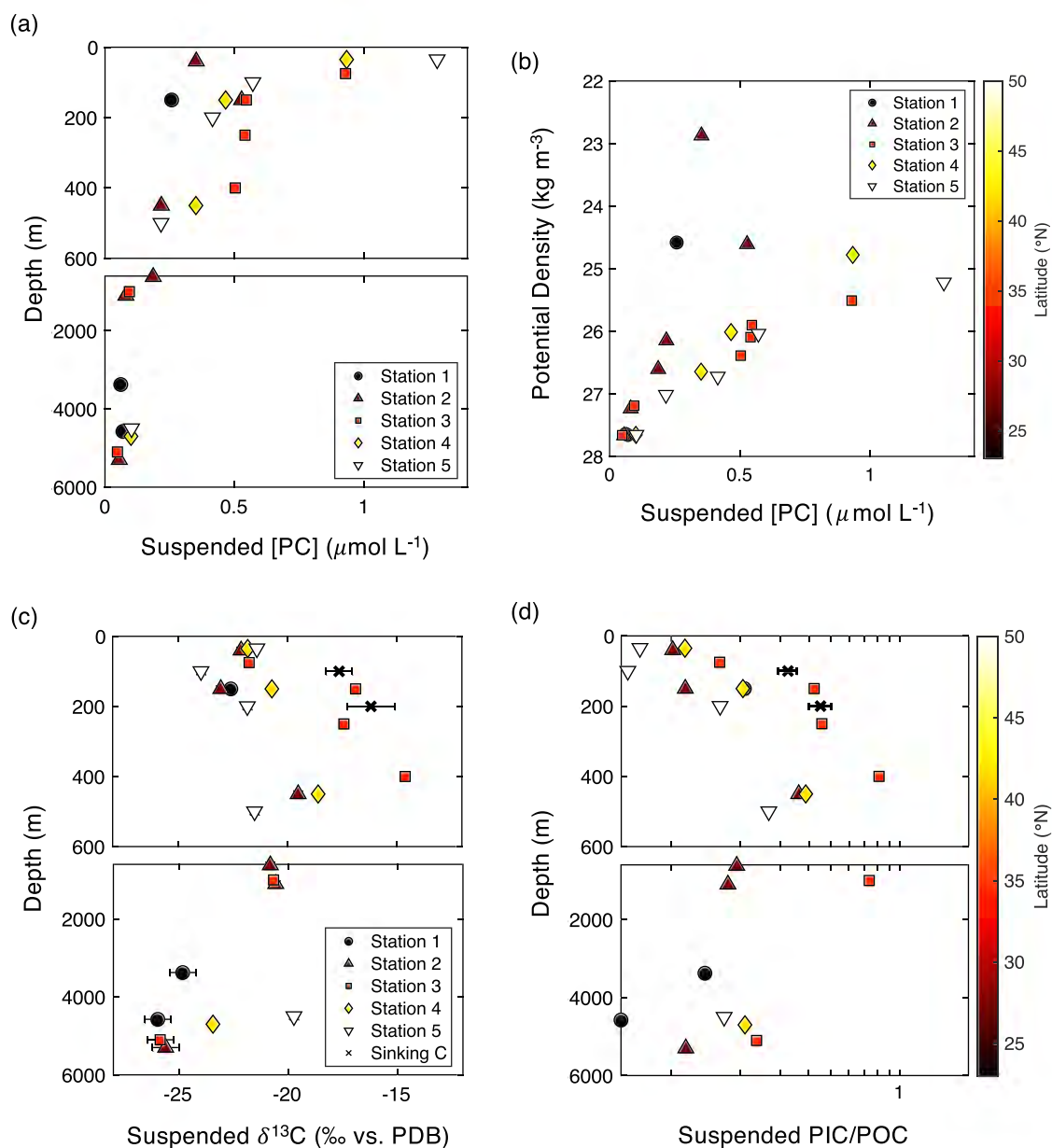
**Fig. 3.** PIC/POC ratio and PC $\delta^{13}$C in suspended particles along the North Pacific transect. **(a)** Suspended total carbon vs. depth for the five stations in CDisK-IV, color coded by latitude. **(b)** Suspended total carbon vs. potential density $\sigma_\theta$. **(c)** Suspended PC $\delta^{13}$C vs. depth. Error bars for the $\delta^{13}$C in deep samples, which have very low total PC content, are estimated based on the standard deviation of $\delta^{13}$C for the EA standards that have similar total C content. The two x's are sinking particles collected in sediment traps, with the error bars representing standard errors among different stations. **(d)** Suspended PIC/POC vs. depth as color-coded symbols. Sediment trap results are plotted as x's to show the sinking PIC/POC. Error bars of x's are standard errors among different stations.

### Analysis of suspended particles

Suspended particles were captured on Advantec GC-50 Glass Fiber Filters (LOT No. 70207718, pore size 0.5 $\mu$m, diameter = 142 mm) through filtration of ~ 1400 L seawater with a dual-flowpath in situ pump (McLane WTS-6-1-142LVUP). Upon recovery, the filters were air-dried and sub-sampled using a hole punch for particulate carbon and nitrogen analyses. PIC content was determined by measuring the amount of $CO_2$ released after acid treatment using an Automate auto-sampler coupled to a G2131-i Picarro Cavity Ring Down spectrometer. Total PC content and $\delta^{13}$C of total PC were measured through combustion in an Elemental Analyzer (Costech) coupled to a Picarro Cavity Ring Down spectrometer. POC was determined as the difference between PC

and PIC. $\delta^{13}C$ of PC was calibrated relative to Pee Dee Belemnite. Based on the reproducibility of $\delta^{13}C$ for the USGS40 standard, our $\delta^{13}C$ measurements have an analytical error of 0.2‰ (1σ) for samples that generate $> 400$ ppm $CO_2$ in the Picarro, and a 1σ uncertainty of ~ 0.6‰ for small size samples. Total PN and $\delta^{15}N$ were measured through combustion using a Thermo Scientific Flash*Smart* Elemental Analyzer coupled to a Delta V Plus Isotope Ratio Mass Spectrometer. $\delta^{15}N$ was calculated relative to air with a precision of 0.2‰ (1σ).

## Results

### Nutrient and $O_2$ concentrations

Nutrient ($NO_3^-$, $PO_4^{3-}$) and $O_2$ concentrations during CDisK-IV are analyzed (Fig. 2; Table S1), and $N^*$, the anomaly of $NO_3^-$ concentration from the photosynthesis/remineralization trend of $16NO_3^-$: $1PO_4^{3-}$, is calculated as $N^* = [NO_3^-] - 16[PO_4^{3-}] + 2.9$ $\mu$mol kg$^{-1}$ (Gruber 2008) (Fig. 2b,c). Surface $NO_3^-$ was below the measurement detection limit at Sta. 1–4 during our cruise in August (Fig. 2a). For $N^*$, Sta. 1–3 show similar patterns in the euphotic zone, and all have positive $N^*$ values in the upper 200 m (Fig. 2b,c), whereas Sta. 4 and 5 (Fig. 2b,c) have low $N^*$ in the shallow water column.

$[O_2]$ measurements during CDisK-IV show that the shallow water column is well oxygenated at Sta. 3 and 4 (Fig. 2d).

### Suspended PC concentration and $\delta^{13}C$

Suspended PC concentrations generally decrease exponentially with depth (Fig. 3a). In the upper 100 m, suspended [PC] is 0.9–1.3 $\mu$mol L$^{-1}$ at the transition zone and in the subarctic gyre, and significantly lower (~ 0.4 $\mu$mol L$^{-1}$) in the subtropical gyre. Below 1000 m, suspended [PC] is $< 0.2$ $\mu$mol L$^{-1}$ for all stations. These values are comparable to previously reported suspended [PC] of ~ 1.7 $\mu$mol L$^{-1}$ in the upper 100 m and ~ 0.08 $\mu$mol L$^{-1}$ below 1000 m in the Eastern Pacific (Lam et al. 2018). The subtropical and subarctic profiles are even more separated out in the [PC] vs. $\sigma_\theta$ plot (Fig. 3b), with more buoyant shallow subtropical water demonstrating both lower $\sigma_\theta$ and lower suspended [PC] than the subarctic. The $\delta^{13}C$ profile of suspended PC increases from the surface to a maximum value at 500 m, and then decreases deeper in the water column (Fig. 3c; Table 1). Because PIC and POC have distinct $\delta^{13}C$ values, $\delta^{13}C$ of PC reflects the relative contribution of PIC and POC. As a result, a similar shape of PC $\delta^{13}C$ is observed in the suspended PIC/POC ratios (Fig. 3d). Sediment trap results are plotted as x's to show the sinking $\delta^{13}C$ and

**Table 1.** Potential density ($\sigma_\theta$), concentrations of PC, PIC, and PN, $\delta^{13}C$ of PC, $\delta^{15}N$ of PN, and $C_{org}$ : N in suspended particles.

| Station | Depth (m) | $\sigma_\theta$ (kg m$^{-3}$) | [PC] ($\mu$mol kg$^{-1}$) | [PIC] ($\mu$mol kg$^{-1}$) | $\delta^{13}C$ (‰) | [PN] ($\mu$mol kg$^{-1}$) | $\delta^{15}N$ (‰) | $C_{org}$ : N |
|---|---|---|---|---|---|---|---|---|
| Sta. 1 | 4575 | 27.7 | 0.069 | 0.0040 | −26.0 | 0.0090 | 7.9 | 7.3 |
| 23°N, | 3375 | 27.6 | 0.061 | 0.0075 | −24.8 | 0.0097 | 8.1 | 5.5 |
| 157°W | 150 | 24.6 | 0.26 | 0.045 | −22.6 | 0.044 | 5.5 | 4.9 |
| Sta. 2 | 5300 | 27.7 | 0.055 | 0.0058 | −25.6 | 0.0088 | 9.7 | 5.6 |
| 28°N, | 1100 | 27.2 | 0.081 | 0.012 | −20.6 | 0.011 | 7.2 | 6.3 |
| 155°W | 620 | 26.6 | 0.19 | 0.030 | −20.8 | 0.026 | 8.6 | 6.0 |
|  | 450 | 26.1 | 0.22 | 0.058 | −19.5 | 0.031 | 8.8 | 5.2 |
|  | 150 | 24.6 | 0.53 | 0.055 | −23.0 | 0.096 | 3.5 | 5.0 |
|  | 40 | 22.9 | 0.35 | 0.033 | −22.1 | 0.053 | 1.0 | 6.1 |
| Sta. 3 | 5100 | 27.7 | 0.048 | 0.0092 | −25.9 | 0.0079 | 9.9 | 5.0 |
| 35°N, | 1000 | 27.2 | 0.094 | 0.040 | −20.7 | 0.015 | 8.6 | 3.7 |
| 150°W | 400 | 26.4 | 0.50 | 0.23 | −14.6 | 0.061 | 10.8 | 4.6 |
|  | 250 | 26.1 | 0.54 | 0.17 | −17.4 | 0.072 | 10.9 | 5.2 |
|  | 150 | 25.9 | 0.55 | 0.16 | −16.9 | 0.074 | 11.2 | 5.2 |
|  | 75 | 25.5 | 0.93 | 0.13 | −21.7 | 0.15 | 9.7 | 5.2 |
| Sta. 4 | 4700 | 27.7 | 0.10 | 0.018 | −23.4 | 0.017 | 11.4 | 5.0 |
| 42°N, | 450 | 26.6 | 0.35 | 0.098 | −18.6 | 0.049 | 10.0 | 5.2 |
| 148°W | 150 | 26.0 | 0.47 | 0.080 | −20.7 | 0.079 | 11.0 | 4.9 |
|  | 35 | 24.8 | 0.93 | 0.096 | −21.8 | 0.23 | 11.5 | 3.7 |
| Sta. 5 | 4500 | 27.7 | 0.10 | 0.015 | −19.7 | 0.021 | 6.8 | 4.3 |
| 50°N, | 500 | 27.0 | 0.22 | 0.046 | −21.5 | 0.044 | 6.0 | 3.9 |
| 149°W | 200 | 26.7 | 0.42 | 0.058 | −21.8 | 0.068 | 6.2 | 5.3 |
|  | 100 | 26.0 | 0.57 | 0.035 | −24.0 | 0.11 | 5.1 | 4.8 |
|  | 35 | 25.2 | 1.3 | 0.087 | −21.4 | 0.25 | 4.4 | 4.9 |

**Fig. 4. (a)** Suspended [PN] vs. depth. **(b)** Suspended $\delta^{15}$N vs. depth. **(c)** Suspended [PN] vs. potential density $\sigma_\theta$.

PIC/POC. Sinking $\delta^{13}$C and PIC/POC are not significantly different among different stations, with the error bars showing the standard errors among stations (Fig. 3c,d). Sinking particles have slightly heavier $\delta^{13}$C and higher PIC/POC than the suspended particles at 100 and 200 m.

**Suspended PN concentration and $\delta^{15}$N**

Suspended PN demonstrate similar profiles as PC, and decrease exponentially with depth (Fig. 4a). Suspended [PN] is 0.2–0.3 $\mu$mol L$^{-1}$ at 35 m in the subarctic gyre, and only 0.05 $\mu$mol L$^{-1}$ at 40 m in the subtropical gyre. Below 1000 m,

suspended [PN] is < 0.02 $\mu$mol L$^{-1}$ for all stations. Suspended $\delta^{15}$N profiles at Sta. 1, 2 (subtropical gyre), and 5 (subarctic gyre) have their lowest value at the surface, and increase with depth until ~ 500 m (Fig. 4b). However, near the transition zone, Sta. 3 and 4 have elevated $\delta^{15}$N of up to 12‰ in the euphotic zone (Fig. 4b; Table 1). Similar to suspended PC, suspended PN also has a different dependence on the potential density $\sigma_\theta$ between the subtropical gyre and the subarctic gyre. The shallow subtropical gyre has lower $\sigma_\theta$ and lower suspended [PN] than the subarctic gyre, but the difference decreases at greater depth (Fig. 4c).

## Discussion

### Water column N* and denitrification along the transect

Based on $NO_3^-$ and $PO_4^{3-}$ concentrations, we calculate N*, the anomaly of $NO_3^-$ concentration from the photosynthesis/remineralization trend of $16NO_3^-$ : $1PO_4^{3-}$, as $N^* = [NO_3^-] - 16[PO_4^{3-}] + 2.9 \mu mol\ kg^{-1}$ (Gruber 2008). Positive N* indicates input of fixed nitrogen through $N_2$ fixation or atmospheric nitrogen deposition whereas negative N* is caused by loss of fixed nitrogen through denitrification or anaerobic ammonium oxidation (anammox). Sta. 1–3 show similar N* patterns in the euphotic zone, and all have positive N* values in the upper 200 m (Fig. 2b,c), consistent with the well-documented $N_2$ fixation feature in the subtropical North Pacific (Karl et al. 1997). The low N* values at Sta. 4 and 5 (Fig. 2b,c) likely reflect a combination of benthic denitrification processes (Christensen et al. 1987; Devol and Christensen 1993; Granger et al. 2011) and the advection of low N* water-column denitrification signal from the Eastern Tropical North Pacific (Sigman et al. 2005). The N* distribution pattern in the upper 600 m determined during CDisK-IV in August matches the pattern determined along the same transect during P16 in March, 2006 (Gruber 2008) and June, 2015 (Macdonald 2015), and demonstrates a relatively steady N* distribution in the North Pacific.

### PIC/POC ratios in suspended particles vs. sinking particles

Particles captured by in situ pumps are usually referred to as suspended particles. These particles span a wide range of sizes; and may sink at different sinking rates depending on their size and density (Lam et al. 2011, 2018). Particles captured by sediment traps are fast-sinking particles including fecal pellet and detrital aggregates. They are generally larger than pump particles and therefore sink faster. We compare the PIC/POC ratios in pump particles and sediment trap particles below. For simplicity, we refer to them as suspended and sinking particles.

The rain ratio, PIC/POC in sinking particles, increases with depth due to the preferential loss of POC as particles settle (Feely et al. 2004; Berelson et al. 2007). In the North Pacific, PIC/POC in sinking particles increases from ~ 0.1 at the surface to ~ 1.6 at 4000 m (Honjo et al. 1995; Rodier and Le Borgne 1997; Wong et al. 1999) (Fig. 5a). On our CDisK-IV cruise, PIC/POC ratios in sinking particles from the upper ocean show no obvious trend among different stations (Dong et al. 2019), and have an average value of $0.32 \pm 0.03$ at 100 m and $0.45 \pm 0.05$ at 200 m (Fig. 5a). These results are consistent with the values observed at Sta. P (Wong et al. 1999) and the Equatorial Pacific (Honjo et al. 1995; Rodier and Le Borgne 1997) (Fig. 5a). Average $\delta^{13}C$ of total PC is $-17.6‰ \pm 0.6‰$ at 100 m, and $-16.2‰ \pm 1.1‰$ at 200 m in the sinking particles (Fig. 3c).

PIC/POC and $\delta^{13}C$ of suspended particles generally agree with these values for sinking particles in the upper 400 m (Figs. 5a, 3c), although the sinking particles have slightly higher PIC/POC and heavier $\delta^{13}C$. Below 500 m, however, PIC/POC in suspended particles starts to decrease with depth, and deviates significantly from the sinking particles (Fig. 5a).

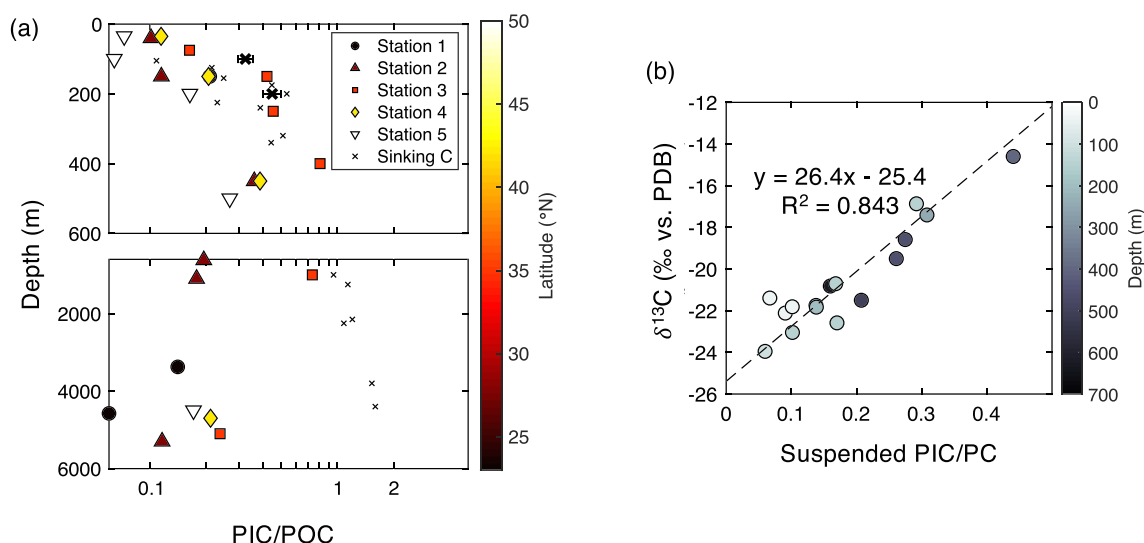This novel feature of different suspended vs. sinking PIC/POC profiles could be due to two possible reasons. First,



**Fig. 5. (a)** Suspended PIC/POC vs. depth as color-coded symbols and sinking PIC/POC as x's. Error bars of x's are standard errors among different stations. Also plotted are previously published sediment trap data in the North Pacific (Honjo et al. 1995; Rodier and Le Borgne 1997; Wong et al. 1999; Dong et al. 2019), these are depicted as small x's. **(b)** Suspended $\delta^{13}C$ vs. PIC/PC in the upper 1000 m. Dashed line is the best fit to the data with a fixed carbonate $\delta^{13}C$ endmember of 1‰.

deep suspended particles may have different residence time than shallow particles and/or come from different environments that are low in PIC. For example, "Brownian pumping" transfers dissolved species to filterable particles through a colloidal intermediate (Honeyman and Santschi 1989), and this process may be a provenance of deep suspended particles that have different PIC/POC feature than the shallow biogenic particles.

The second possible explanation of the discrepancy between suspended and sinking PIC/POC is the relative importance of POC remineralization and PIC dissolution at different depths of the water column. In the euphotic zone, suspended particles of biogenic phases are primarily supplied through production, and aggregate into sinking particles which sink below the mixed layer. At depths that are > 100 m below the euphotic zone, disaggregation dominates aggregation processes, and suspended particles are generated from semi-decomposed sinking particles (Lam et al. 2018). Therefore, the fact that suspended particles have higher POC fraction relative to PIC fraction than sinking particles in the shallow water column (upper 200 m) is likely due to the sinking of the particles containing higher ballast (PIC) percentage after the physical break-down of the biomass, leaving the remaining part higher in POC percentage; or the preferential sinking of particles with high PIC percentage in themselves (i.e., pteropods and foraminifera). The deviation of suspended PIC/POC from sinking particles below 500 m

could potentially reflect PIC dissolution as sinking particles decompose to become smaller suspended particles. Interestingly, we do not observe lower PIC/POC or lighter $\delta^{13}C$ at higher latitudes, which have a more under-saturated water column for $CaCO_3$ than the lower latitude stations. The saturation horizon for calcite is around 750 m for Sta. 1, and 350 m for Sta. 5; whereas the saturation horizon for aragonite is around 550 m for Sta. 1, and only 150 m for Sta. 5 (Dong et al. 2019; Naviaux et al. 2019). However, except for Sta. 3 which has an elevated PIC pool in the intermediate depth (100–800 m), the other four stations exhibit the same suspended PIC/POC profile vs. depth. This may imply that PIC dissolution within the particles is insensitive to the water column $\Omega$, but rather depends on the local water chemistry in particle micro-environments, which is largely affected by organic matter respiration (Jansen et al. 2002; Bianchi et al. 2018; Dong et al. 2019), or the metabolic activity of zooplankton which may promote dissolution through grazing and digestion (Milliman et al. 1999; Jansen and Wolf-Gladrow 2001).

$\delta^{13}C$ of total PC scales reasonably linearly with PIC/PC for the suspended particles in the upper 1000 m (Fig. 5b). Assuming that the carbonate endmember has a $\delta^{13}C$ value of 1‰, fitting the $\delta^{13}C$ vs. PIC/PC data yields a POC $\delta^{13}C$ endmember of −25.4‰. This average POC $\delta^{13}C$ is consistent with widely accepted $\delta^{13}C$ value of ∼ −25‰ in most marine plankton populations (Hansman and Sessions 2016).
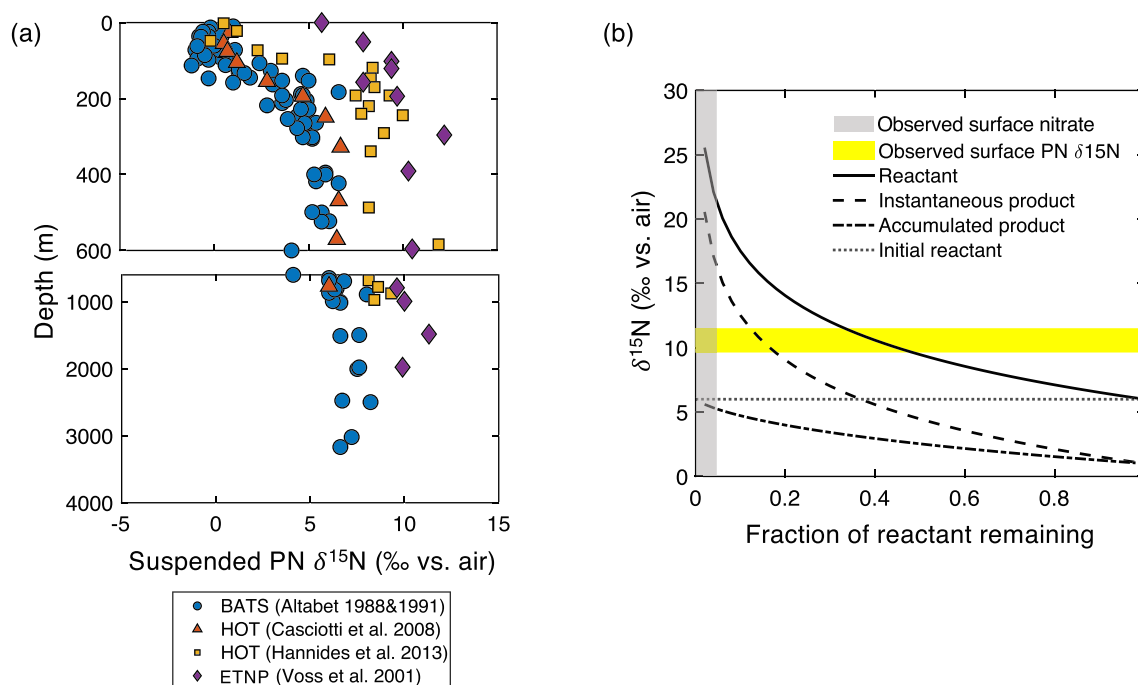


**Fig. 6. (a)** Previously published profiles of suspended $\delta^{15}N$. **(b)** Rayleigh fractionation during the consumption of nitrate in a closed pool. The reactant is nitrate, and the product is PN. Shaded yellow area represents the observed surface suspended PN $\delta^{15}N$ at Sta. 3 and 4 ($\delta^{15}N$ = 9.7‰ at 75 m in Sta. 3, and 11.5‰ at 35 m in Sta. 4). Shaded gray area represents observed nitrate remaining at the surface (*see* Fig. 1 for details).

**Suspended PN $\delta^{15}$N**

A typical depth profile of suspended particle $\delta^{15}$N has its lowest value at the surface, and increases with depth until ~500 m (Sigman and Fripiat 2019). This typical $\delta^{15}$N profile has been reported at BATS (Altabet 1988; Altabet et al. 1991), HOT (Casciotti et al. 2008; Hannides et al. 2013) and the ETNP (Voss et al. 2001) (Fig. 6a). For example, in the subtropical North Atlantic Ocean near BATS, $\delta^{15}$N is −1‰ to 1‰ at the surface, increases to 7–8‰ at ~500 m, and stays relatively constant below 500 m (Altabet et al. 1991). Along our North Pacific transect, $\delta^{15}$N profiles at Sta. 1, 2 (subtropical gyre), and 5 (subarctic gyre) are in good agreement with the typical suspended $\delta^{15}$N profiles in the tropical–subtropical ocean (Fig. 4b). However, near the transition zone, Sta. 3 and 4 deviate from the expected trend, with elevated $\delta^{15}$N of up to 12‰ observed in the euphotic zone (Fig. 4b; Table 1).

In the euphotic zone, $\delta^{15}$N in the suspended particles reflects the $\delta^{15}$N of new nitrogen supply (e.g., either the upwelling of thermocline nitrate or N$_2$ fixation), as well as subsequent N fractionating processes within the euphotic zone (Sigman and Fripiat 2019). In the (sub)tropical oceans, suspended particle $\delta^{15}$N in the surface ocean is typically 2–3‰ lower than the $\delta^{15}$N of thermocline nitrate or sinking particles due to N recycling (Casciotti et al. 2008; Fawcett et al. 2011; Yang et al. 2017). At BATS and HOT, the surface suspended $\delta^{15}$N are −1 to 1‰ (Fig. 6a) (Altabet 1988; Casciotti et al. 2008). In the Eastern Tropical South Pacific where the thermocline nitrate $\delta^{15}$N (10–11‰) is elevated by water-column denitrification, the euphotic zone suspended $\delta^{15}$N are 8–10‰ (Knapp et al. 2016). Thermocline nitrate $\delta^{15}$N at Sta. 3 and 4 are ~6‰ based on GEOTRACES-GP15 data (D. Marconi et al. unpubl.). Thus, the expected surface suspended $\delta^{15}$N should be 3–4‰ for Sta. 3 and 4, which is inconsistent with our observed unusually high suspended PN $\delta^{15}$N.

During nitrate uptake, phytoplankton preferentially assimilate $^{14}$N relative to $^{15}$N. As a result, the $\delta^{15}$N of the remaining nitrate pool gradually increases as nitrate consumption proceeds and nitrate concentration decreases. The Rayleigh model is often used to simulate the uptake of nitrate by phytoplankton during high-productivity periods. The Rayleigh fractionation kinetics define the isotopic variation of the reactant N
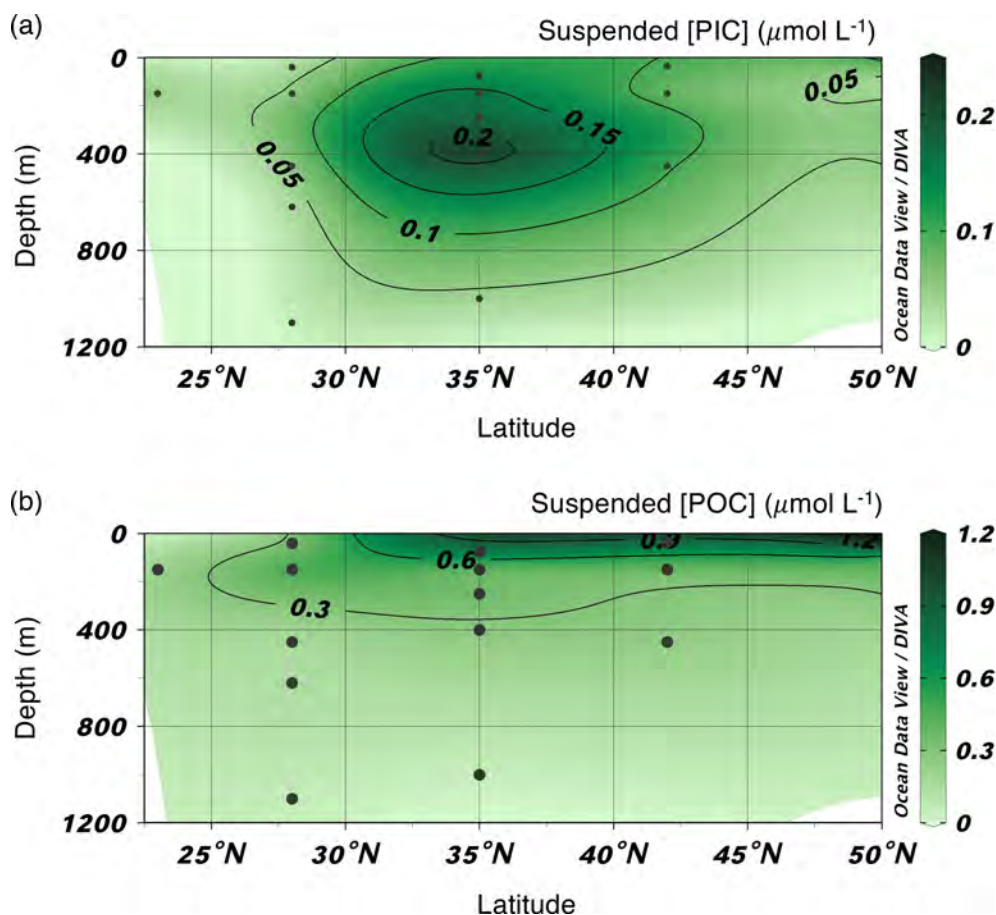


**Fig. 7.** Suspended PIC and POC concentrations in the upper 1200 m along the CDisK-IV transect. **(a)** Suspended [PIC] determined by a Picarro laser spectrometer. The "bullseye" pattern in the intermediate depth (150–500 m) at Sta. 3 is also verified by mineralogy analysis using Raman spectroscopy. **(b)** Suspended [POC] determined by subtracting [PIC] from [PC]. Total suspended [PC] is determined by EA analysis.

pool, the instantaneously generated product, and the accumulated product N pool as the given reservoir of reactant N is consumed (Sigman and Fripiat 2019). Using a starting nitrate $\delta^{15}N$ of 6‰ for Sta. 3 and 4 (Rafter et al. 2019; D. Marconi et al. unpubl.) and an isotope effect of 5‰ for nitrate assimilation (Sigman and Fripiat 2019), we have calculated the $\delta^{15}N$ of accumulated PN and instantaneous PN (Fig. 6b). The remaining surface nitrate concentration at Sta. 3 and 4 is close to zero such that the accumulated PN $\delta^{15}N$ should approach the $\delta^{15}N$ of the starting nitrate. However, the observed PN $\delta^{15}N$ is 4–5‰ higher than the $\delta^{15}N$ of the accumulated PN, indicating the PN we analyzed cannot be the accumulated PN pool. Rather, these high suspended PN $\delta^{15}N$ values require that the previously accumulated low-$\delta^{15}N$ biomass (i.e., relative to the subsurface nitrate $\delta^{15}N$) during the phytoplankton bloom would have been mostly exported out of the euphotic zone. Thus the suspended PN we captured only represents the remaining biomass in the euphotic zone.

Our interpretation is also consistent with the previous observations of seasonally and locally high suspended PN $\delta^{15}N$ when the biological uptake rate of nitrate is greater than the physical supply (Voss et al. 1996; Wu et al. 1997). Specifically, an increase in suspended $\delta^{15}N$ between June and September, and a decrease toward November was reported in the Lofoten Basin, off-coast of Norway (Voss et al. 1996). The elevated suspended PN $\delta^{15}N$ in September was related to the instantaneous product during nitrate uptake and fractionation. On a transect between a coastal upwelling domain and Sta. P, suspended PN $\delta^{15}N$ was found to increase rapidly where biological uptake of nitrate is greater than the physical supply, and it decreases during upwelling events when physical supply of nutrients overwhelms the biological uptake rate (Wu et al. 1997).

A surface production bloom at Sta. 3 prior to CDisK-IV is supported by suspended PC data in addition to $\delta^{15}N$. The high suspended [PC] in the intermediate depth (150–500 m) at Sta. 3 (Fig. 3a) is due to an abnormally high suspended PIC concentration (Fig. 7a), supported by both total PIC analysis using a Picarro laser spectrometer and mineralogy analysis using Raman spectroscopy (Dong et al. 2019). The "bullseye" pattern at this location in suspended PIC (Fig. 7a), however, is not observed in suspended POC (Fig. 7b). We propose that PIC produced during the previous weeks to months before CDisK-IV when the TZCF resided near that latitude has not been totally dissolved, but POC has a shorter residence time and has been decomposed (Dong et al. 2019).

The $N^*$ and $O_2$ concentrations can be used to further test whether the shallow water column at Sta. 3 and 4 has more pronounced denitrification signals than the other stations (Fig. 2; Table S1). As discussed in Discussion 4.1, the $N^*$ distribution pattern in the upper 600 m determined during CDisK-IV in August matches the pattern determined along the same transect during P16 in March, 2006 (Gruber 2008) and June, 2015 (Macdonald 2015), and demonstrates a relatively steady

$N^*$ spatial distribution in the North Pacific. As a result, the shallow water column at Sta. 3 and 4 do not show more pronounced denitrification signals than the other stations (Fig. 2; Table S1). No obvious local denitrification beneath the high productivity regions in the transition zone is observed. In addition, $[O_2]$ measurements during CDisK-IV show that the shallow water column is well oxygenated at Sta. 3 and 4 (Fig. 2d), further disproving denitrification at these locations.

The elevated suspended PN $\delta^{15}N$ has implications for the upper ocean nitrogen cycling in oligotrophic waters. On an annual basis (Fig. 8a), the primary production in the oligotrophic North Pacific is mainly fueled by the recycled ammonium ("recycled production"). Low-$\delta^{15}N$ ammonium is produced in the surface ocean due to the isotopic effect of amino acid catabolism in zooplankton (Sigman and Fripiat 2019). Phytoplankton then assimilate the low-$\delta^{15}N$ ammonium and generate low-$\delta^{15}N$ suspended PN, while sinking particles preferentially export relatively higher-$\delta^{15}N$ PN out of the euphotic zone. Recently, isotopic analyses of flow cytometry sorted cells in the Sargasso Sea showed that small eukaryotes in the surface ocean have higher $\delta^{15}N$ than cyanobacteria because they directly assimilate the upwelled nitrate (Fawcett et al. 2011). These eukaryotes with higher $\delta^{15}N$ could be responsible for the export of high-$\delta^{15}N$ nitrogen as they represent a more significant fraction of the sinking PN through sinking aggregate incorporation or fecal pellet packaging (Fawcett et al, 2011).

In contrast, during a phytoplankton bloom (Fig. 8b), nitrate supplied during winter mixing, rather than the recycled ammonium, becomes the dominant source of nitrogen for phytoplankton growth. As small eukaryotes are mainly responsible for nitrate assimilation and they tend to sink out of the euphotic zone through fecal pellets or aggregates (Fawcett et al. 2011), the sinking PN fluxes are higher than the mean annual scenario (Fig. 8a). In addition, these sinking PN have lower $\delta^{15}N$ than the subsurface nitrate because of the Rayleigh fractionation (Fig. 6b). As a result, the $\delta^{15}N$ of the remaining suspended PN in the euphotic zone could be higher than the subsurface nitrate $\delta^{15}N$.

## $C_{org}$ : N molar ratio in suspended particles

Measured suspended [POC] and [PN] show a highly linear correlation, with an average $C_{org}$ : N molar ratio of 4.59 (Fig. 9a). $C_{org}$ : N ratios vary between 3.7 and 7.3 (Table 1), and have an average value of $5.1 \pm 0.2$, lower than the canonical Redfield $C_{org}$ : N ratio of 6.6 (Fig. 9b). Our measured suspended $C_{org}$ : N ratios generally follow a normal distribution, with 62.5% of the ratios lying between 5 and 6 (Fig. 9c). At the deep chlorophyll maximum at Sta. 1 (ALOHA), our measured suspended $C_{org}$ : N ratio of 5.9 matches well with previously reported $C_{org}$ : N value of ~ 6 for < 51-$\mu$m particles and ~ 5 for > 51-$\mu$m particles at the same location and depth (Bishop and Wood 2008). At Sta. 5 (Sta. P), our suspended $C_{org}$ : N ratios of 5.2 at 35 m and 5.1 at 100 m also match well
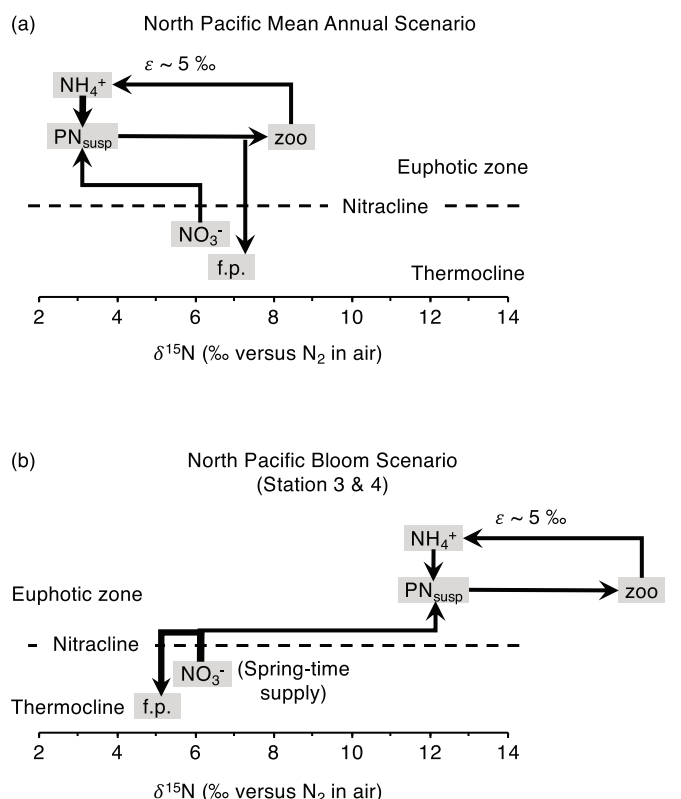
**Fig. 8.** N Fluxes and their $\delta^{15}$N in the oligotrophic North Pacific $\delta^{15}$N. **(a)** Mean annual scenario. New N source (subsurface nitrate) has a $\delta^{15}$N of ~6‰. Recycled N (ammonium) is 5‰ lower than zooplankton (zoo) $\delta^{15}$N. Export fluxes, which include fecal pellet (f.p.) and detrital aggregates, have slightly higher $\delta^{15}$N than the nitrate supply based on mass balance. **(b)** Bloom scenario. Export $\delta^{15}$N becomes lower than $\delta^{15}$N of the nitrate supply. Recycled N supply becomes less significant than nitrate supply, which gives higher ef-ratio ($\frac{\text{new production}}{\text{new+regenerated production}}$) during the bloom/high-production scenario (Van Oostende et al. 2015; Laws et al. 2011).



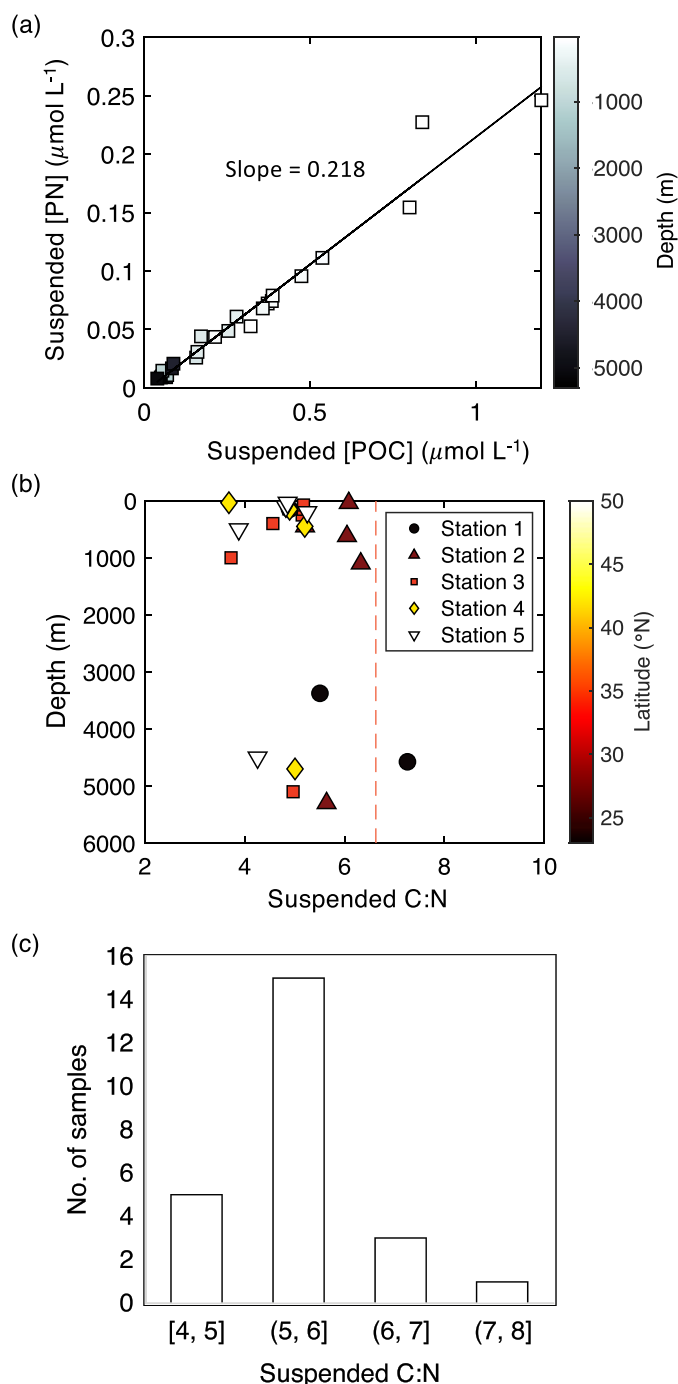**Fig. 9.** $C_{org} : N$ molar ratio in the suspended particles along the North Pacific transect. **(a)** Suspended [POC] vs. [PN]. **(b)** Suspended $C_{org} : N$ molar ratio vs. depth for the five stations. Red dashed line indicates the canonical Redfield ratio of $C_{org} : N = 6.6$. **(c)** Distribution of suspended $C_{org} : N$ molar ratios.

with previously reported $C_{org} : N$ in the upper 100 m (mean = 5.4) (Minagawa et al. 2001), but our suspended $C_{org} : N$ disagrees with theirs below 1000 m (mean = 9.1). Along the same longitude at the equator, $C_{org} : N$ was also shown to be low (mean = 5.9) in the upper 320 m (Rodier and Le Borgne 1997). In the North Pacific Western Subarctic Gyre, suspended $C_{org} : N$ was shown to be 5.9 at 0–50 m, and 7.2 at 100–200 m (Mino et al. 2016).

$C_{org} : N$ molar ratios on suspended particles > 1000 m are slightly higher than at shallower depths (Fig. 9b), consistent with the trend previously reported at Stat. P (Minagawa et al. 2001) and the Eastern Pacific (Lam et al. 2018), even though our $C_{org} : N$ ratios are smaller. The higher suspended $C_{org} : N$ ratios at deeper depth may reflect a preferable loss of N during remineralization, or different sources of shallow and deep particles. A higher $C_{org} : N$ ratio is observed in the subtropical gyre ($C_{org} : N = 5.8 \pm 0.3$) compared to the transition zone

($C_{org} : N = 4.8 \pm 0.2$) and the subarctic gyre ($C_{org} : N = 4.6 \pm 0.2$), consistent with the mean global trend that warm nutrient-depleted low latitude gyres have a higher average

$C_{org}$ : N (mean $C_{org}$ : N = 7.0) than the cold nutrient-rich high latitude regions (mean $C_{org}$ : N = 6.0) (Martiny et al. 2013).

## Conclusion

We present PIC/POC ratios in suspended particles along a North Pacific transect, and show a deviation between settling and suspended PIC/POC below 600 m. The discrepancy is likely due to the different provenance of deep suspended particles than shallow biogenic sources, or PIC dissolution within suspended particles. Isotope balance gives a POC $\delta^{13}C$ of −25.4‰, assuming a PIC $\delta^{13}C$ of 1‰. This value of $\delta^{13}C$ is consistent across a wide range of the N. Pacific and through a range of $C_{org}$ : N values for POM. $\delta^{15}N$ of suspended particles in the subtropical and subarctic gyres follow typical depth profiles, with low $\delta^{15}N$ in the euphotic zone and high $\delta^{15}N$ at depth. However, highly elevated suspended PN $\delta^{15}N$ values were observed in the euphotic zone near the transition zone, likely caused by the export of low-$\delta^{15}N$ PN during the phytoplankton bloom. This export process was probably facilitated by small eukaryotes. Finally, suspended $C_{org}$ : N ratios along the North Pacific transect are generally lower than the canonical value, with an average of 5.1 ± 0.2. The subtropical gyre has slightly higher suspended $C_{org}$ : N ratios than the transition zone and the subarctic gyre. Deep suspended $C_{org}$ : N ratios are higher than shallow ratios.

## References

Altabet, M. A. 1988. Variations in nitrogen isotopic composition between sinking and suspended particles: Implications for nitrogen cycling and particle transformation in the open ocean. Deep Sea Res. Part A Oceanogr. Res. Pap. **35**: 535–554. doi:10.1016/0198-0149(88)90130-6

Altabet, M. A., W. G. Deuser, S. Honjo, and C. Stienent. 1991. Seasonal and depth-related changes in the source of sinking particles in the North Atlantic. Nature **354**: 136–139.

Altabet, M. A., C. Pilskaln, R. Thunell, C. Pride, D. Sigman, F. Chavez, and R. Francois. 1999. The nitrogen isotope biogeochemistry of sinking particles from the margin of the eastern North Pacific. Deep Sea Res. Part 1 Oceanogr. Res. Pap. **46**: 655–679. doi:10.1016/S0967-0637(98)00084-3

Armstrong, R. A., C. Lee, J. I. Hedges, S. Honjo, and S. G. Wakeham. 2002. A new, mechanistic model for organic carbon fluxes in the ocean based on the quantitative association of POC with ballast minerals. Deep-Sea Res. Part II Topical Stud. Oceanogr. **49**: 219–236. doi:10.1016/S0967-0645(01)00101-1

Ayers, J. M., and M. Susan Lozier. 2010. Physical controls on the seasonal migration of the North Pacific transition zone chlorophyll front. J. Geophys. Res. Oceans **115**: 1–11. doi:10.1029/2009JC005596

Berelson, W. M., W. M. Balch, R. Najjar, R. A. Feely, C. Sabine, and K. Lee. 2007. Relating estimates of CaCO₃ production,

export, and dissolution in the water column to measurements of CaCO₃ rain into sediment traps and dissolution on the sea floor: A revised global carbonate budget. Global Biogeochem. Cycles **21**: 1–15. doi:10.1029/2006GB002803

Bianchi, D., T. S. Weber, R. Kiko, and C. Deutsch. 2018. Global niche of marine anaerobic metabolisms expanded by particle microenvironments. Nat. Geosci. **11**: 1–6. doi:10.1038/s41561-018-0081-0

Bishop, J. K. B., and T. J. Wood. 2008. Particulate matter chemistry and dynamics in the twilight zone at VERTIGO ALOHA and K2 sites. Deep Sea Res. Part 1 Oceanogr. Res. Pap. **55**: 1684–1706. doi:10.1016/j.dsr.2008.07.012

Bograd, S. J., D. G. Foley, F. B. Schwing, R. Cara Wilson, M. Laurs, J. J. Polovina, E. A. Howell, and R. E. Brainard. 2004. On the seasonal and interannual migrations of the transition zone chlorophyll front. Geophys. Res. Lett. **31**: 1–5. doi:10.1029/2004GL020637

Casciotti, K. L., T. W. Trull, D. M. Glover, and D. Davies. 2008. Constraints on nitrogen cycling at the subtropical North Pacific Station ALOHA from isotopic measurements of nitrate and particulate nitrogen. Deep-Sea Res. Part II Topical Stud. Oceanogr. **55**: 1661–1672. doi:10.1016/j.dsr2.2008.04.017

Christensen, J. P., J. W. Murray, A. H. Devol, and L. A. Codispoti. 1987. Denitrification in continental shelf sediments has major impact on the oceanic nitrogen budget. Global Biogeochem. Cycles **1**: 97–116.

Conkright, M E, R A Locarnini, H E Garcia, T D O'Brien, T P Boyer, C Stepens, and J I Antonov. 2002. "World Ocean Atlas 2001: Objective analyses, data statistics, and figures CD-ROM documentation." National Oceanographic Data Center Internal Report (NOAA Atlas NESDIS), Silver Spring, MD.

Devol, A. H., and J. P. Christensen. 1993. Benthic fluxes and nitrogen cycling in sediments of the continental margin of the eastern North Pacific. J. Mar. Res. **51**: 345–372. doi:10.1357/0022240933223765

Devries, T., and C. Deutsch. 2014. Large-scale variations in the stoichiometry of marine organic matter respiration. Nat. Geosci. **7**: 890–894. doi:10.1038/ngeo2300

Dong, S., and others. 2019. Aragonite dissolution kinetics and calcite/aragonite ratios in sinking and suspended particles in the North Pacific. Earth Planet. Sci. Lett. **515**: 1–12. doi:10.1016/j.epsl.2019.03.016

Eguchi, N. O., H. Ujiié, H. Kawahata, and A. Taira. 2003. Seasonal variations in planktonic foraminifera at three sediment traps in the subarctic, transition and subtropical zones of the central North Pacific Ocean. Marine Micropaleontol. **48**: 149–163. doi:10.1016/S0377-8398(03)00020-3

Fawcett, S. E., M. W. Lomas, J. R. Casey, B. B. Ward, and D. M. Sigman. 2011. Assimilation of upwelled nitrate by small eukaryotes in the Sargasso Sea. Nat. Geosci. **4**: 717–722. doi:10.1038/ngeo1265

Feely, R. A., C. L. Sabine, R. Schlitzer, J. L. Bullister, S. Mecking, and D. Greeley. 2004. Oxygen utilization and organic carbon remineralization in the upper water column

of the Pacific Ocean. J. Oceanogr. **60**: 45–52. doi:10.1023/B:JOCE.0000038317.01279.aa

Granger, J., M. G. Prokopenko, D. M. Sigman, C. W. Mordy, Z. M. Morse, L. V. Morales, R. N. Sambrotto, and B. Plessen. 2011. Coupled nitrification-denitrification in sediment of the eastern Bering Sea shelf leads to ${}^{15}$N enrichment of fixed N in shelf waters. J. Geophys. Res. Oceans **116**: 1–18. doi:10.1029/2010JC006751

Gruber, N. 2008. The marine nitrogen cycle: Overview and challenges. *In* Nitrogen in the Marine Environment, v. **1–50**. Academic Press. doi:10.1016/B978-0-12-372522-6.00001-3

Gruber, N., and J. L. Sarmiento. 1997. Global patterns of marine nitrogen fixation and denitrification. Global Biogeochem. Cycles **11**: 235–266.

Hannides, C. C. S., B. N. Popp, C. Anela Choy, and J. C. Drazen. 2013. Midwater zooplankton and suspended particle dynamics in the North Pacific subtropical gyre: A stable isotope perspective. Limnol. Oceanogr. **58**: 1931–1946. doi:10.4319/lo.2013.58.6.1931

Hansman, R. L., and A. L. Sessions. 2016. Measuring the in situ carbon isotopic composition of distinct marine plankton populations sorted by flow cytometry. Limnol. Oceanogr.: Methods **14**: 87–99. doi:10.1002/lom3.10073

Honeyman, B. D., and P. H. Santschi. 1989. A Brownian-pumping model for oceanic trace metal scavenging: Evidence from Th isotopes. J. Mar. Res. **47**: 951–992. doi:10.1357/002224089785076091

Honjo, S., J. Dymond, R. Collier, and S. J. Manganini. 1995. Export production of particles to the interior of the equatorial Pacific Ocean during the 1992 EqPac experiment. Deep-Sea Res. Part II **42**: 831–870. doi:10.1016/0967-0645(95)00034-N

Honjo, S., S. J. Manganini, R. A. Krishfield, and R. Francois. 2008. Particulate organic carbon fluxes to the ocean interior and factors controlling the biological pump: A synthesis of global sediment trap programs since 1983. Prog. Oceanogr. **76**: 217–285. doi:10.1016/j.pocean.2007.11.003

Hou, Y., D. E. Hammond, W. M. Berelson, N. Kemnitz, J. F. Adkins, and A. Lunstrum. 2019. Spatial patterns of benthic silica flux in the North Pacific reflect upper ocean production. Deep Sea Res. Part 1 Oceanogr. Res. Pap. **148**: 25–33. doi:10.1016/j.dsr.2019.04.013

Jansen, H., and D. A. Wolf-Gladrow. 2001. Carbonate dissolution in copepod guts: a numerical model. Marine Ecology Progress Series **221**: 199–207.

Jansen, H., R. E. Zeebe, and D. A. Wolf-Gladrow. 2002. Modeling the dissolution of settling $CaCO_3$ in the ocean. Global Biogeochem. Cycles **16**: 11. doi:10.1029/2000gb001279

Jokulsdottir, T., and D. Archer. 2015. A stochastic, Lagrangian model of sinking biogenic aggregates in the ocean (SLAMS 1.0): Model formulation, validation and sensitivity. Geosci. Model Develop. Discuss. **8**: 5931–5982. doi:10.5194/gmdd-8-5931-2015

Juranek, L. W., P. D. Quay, R. A. Feely, D. Lockwood, D. M. Karl, and M. J. Church. 2012. Biological production in the NE Pacific and its influence on air-sea $CO_2$ flux: Evidence from dissolved oxygen isotopes and O 2/Ar. J. Geophys. Res. Oceans **117**: 1–23. doi:10.1029/2011JC007450

Karl, D., R. Letelier, L. Tupas, J. Dore, J. Christian, and D. Hebel. 1997. The role of nitrogen fixation in biogeochemical cycling in the subtropical North Pacific Ocean. Nature **388**: 533–538. doi:10.1038/41474

Kawahata. 1998. Sinking particles between the equatorial and subarctic regions (0N-46N) in the Central Pacific. Geochem. J. **32**: 125–133.

Klaas, C., and D. E. Archer. 2002. Association of Sinking Organic Matter with various types of mineral ballast in the deep sea: Implications for the rain ratio. Global Biogeochem. Cycles **16**: 63. doi:10.1029/2001gb001765

Knapp, A. N., K. L. Casciotti, W. M. Berelson, M. G. Prokopenko, and D. G. Capone. 2016. Low rates of nitrogen fixation in eastern tropical South Pacific surface waters. Proc. Natl. Acad. Sci. U. S. A. **113**: 4398–4403. doi:10.1073/pnas.1515641113

Lam, P. J., S. C. Doney, and J. K. B. Bishop. 2011. The dynamic ocean biological pump: Insights from a global compilation of particulate organic carbon, $CaCO_3$, and opal concentration profiles from the mesopelagic. Global Biogeochem. Cycles **25**: 1–14. doi:10.1029/2010GB003868

Lam, P. J., J. M. Lee, M. I. Heller, S. Mehic, Y. Xiang, and N. R. Bates. 2018. Size-fractionated distributions of suspended particle concentration and major phase composition from the U.S. GEOTRACES Eastern Pacific Zonal Transect (GP16). Mar. Chem. **201**: 90–107. doi:10.1016/j.marchem.2017.08.013

Laws, E. A., E. D'Sa, and P. Naik. 2011. Simple equations to estimate ratios of new or export production to Total production from satellite-derived estimates of sea surface temperature and primary production. Limnol. Oceanogr.: Methods **9**: 593–601. doi:10.4319/lom.2011.9.593

Macdonald, A. 2015. P16N/2 2015 [Data Set]. CCHDO: CLIVAR and Carbon Hydrographic Data Office. doi:10.7942/C2RP43.

Martiny, A. C., C. T. A. Pham, F. W. Primeau, J. A. Vrugt, J. Keith Moore, S. A. Levin, and M. W. Lomas. 2013. Strong latitudinal patterns in the elemental ratios of marine plankton and organic matter. Nat. Geosci. **6**: 279–283. doi:10.1038/ngeo1757

Milliman, J. D., P. J. Troy, W. M. Balch, A. K. Adams, Y. H. Li, and F. T. Mackenzie. 1999. Biologically mediated dissolution of calcium carbonate above the chemical Lysocline? Deep Sea Res. Part 1 Oceanogr. Res. Pap. **46**: 1653–1669. doi:10.1016/S0967-0637(99)00034-5

Minagawa, M., M. Ohashi, T. Kuramoto, and N. Noda. 2001. Δ15N of PON and nitrate as a clue to the origin and transformation of nitrogen in the subarctic North Pacific and its marginal sea. J. Oceanogr. **57**: 285–300. doi:10.1023/A:1012430512137

Mino, Y., C. Sukigara, M. C. Honda, H. Kawakami, K. Matsumoto, M. Wakita, M. Kitamura, and others. 2016. Seasonal variations in the nitrogen isotopic composition of settling particles at station K2 in the Western subarctic North Pacific. J. Oceanogr. **72**: 819–836. doi:10.1007/s10872-016-0381-1

Naviaux, J. D., A. V. Subhas, S. Dong, N. E. Rollins, X. Liu, R. H. Byrne, W. M. Berelson, and J. F. Adkins. 2019. Calcite dissolution rates in seawater: Lab vs. in-situ measurements and inhibition by organic matter. Mar. Chem. **215**: 103684. doi:10.1016/j.marchem.2019.103684

Oostende, N., J. P. Van, S. E. Dunne, and Fawcett, and B. B. Ward. 2015. Phytoplankton succession explains size-partitioning of new production following upwelling-induced blooms. J. Mar. Syst. **148**: 14–25. doi:10.1016/j.jmarsys.2015.01.009

Polovina, J. J., E. A. Howell, D. R. Kobayashi, and M. P. Seki. 2017. The transition zone chlorophyll front updated: Advances from a decade of research. Prog. Oceanogr. **150**: 79–85. doi:10.1016/j.pocean.2015.01.006

Polovina, J. J., E. Howell, D. R. Kobayashi, and M. P. Seki. 2001. The transition zone chlorophyll front, a dynamic global feature defining migration and forage habitat for marine resources. Prog. Oceanogr. **49**: 469–483. doi:10.1016/S0079-6611(01)00036-2

Rafter, P. A., A. Bagnell, D. Marconi, and T. DeVries. 2019. Global trends in marine nitrate N isotopes from observations and a neural network-based climatology. Biogeosciences Discussions **16**: 2617–2633. doi:10.5194/bg-2018-525

Rodier, M., and R. Le Borgne. 1997. Export flux of particles at the equator in the Western and Central Pacific Ocean. Deep-Sea Res. Part II Top. Stud. Oceanogr. **44**: 2085–2113. doi:10.1016/S0967-0645(97)00092-1

Sarmiento, J. L., J. Dunne, A. Gnanadesikan, R. M. Key, K. Matsumoto, and R. Slater. 2002. A new estimate of the CaCO 3 to organic carbon export ratio. Global Biogeochem. Cycles **16**: 54. doi:10.1029/2002gb001919

Sigman, D. M., and F. Fripiat. 2019. Nitrogen isotopes in the ocean, p. 263–278. *In* Encyclopedia of Ocean Sciences. Elsevier. doi:10.1016/B978-0-12-409548-9.11605-7

Sigman, J. G., P. J. DiFiore, M. M. Lehmann, R. Ho, G. Cane, and A. van Geen. 2005. Coupled nitrogen and oxygen isotope measurements of nitrate along the eastern North Pacific margin. Global Biogeochem. Cycles **19**: 1–14. doi:10.1029/2005GB002458

Teng, Y. C., F. W. Primeau, J. Keith Moore, M. W. Lomas, and A. C. Martiny. 2014. Global-scale variations of the ratios of carbon to phosphorus in exported marine organic matter. Nat. Geosci. **7**: 895–898. doi:10.1038/ngeo2303

Voss, M., M. A. Altabet, and B. V. Bodungen. 1996. Δ15N in sedimenting particles as indicator of euphotic-zone processes. Deep Sea Res. Part 1 Oceanogr. Res. Pap. **43**: 33–47. doi:10.1016/0967-0637(95)00099-2

Voss, M., J. W. Dippner, and J. P. Montoya. 2001. Nitrogen isotope patterns in the oxygen-deficient waters of the eastern tropical North Pacific Ocean. Deep Sea Res. Part 1 Oceanogr. Res. Pap. **48**: 1905–1921. doi:10.1016/S0967-0637(00)00110-2

Wong, C. S., F. A. Whitney, D. W. Crawford, K. Iseki, R. J. Matear, W. K. Johnson, J. S. Page, and D. Timothy. 1999. Seasonal and interannual variability in particle fluxes of carbon, nitrogen and silicon from time series of sediment traps at Ocean Station P, 1982-1993: Relationship to changes in subarctic primary productivity. Deep-Sea Res. Part II Top. Stud. Oceanogr. **46**: 2735–2760. doi:10.1016/S0967-0645(99)00082-X

Wu, J., S. E. Calvert, and C. S. Wong. 1997. Nitrogen isotope variations in the subarctic Northeast Pacific: Relationships to nitrate utilization and trophic structure. Deep Sea Res. Part 1 Oceanogr. Res. Pap. **44**: 287–314. doi:10.1016/S0967-0637(96)00099-4

Yamaguchi, Y. T., and M. D. McCarthy. 2018. Sources and transformation of dissolved and particulate organic nitrogen in the North Pacific subtropical gyre indicated by compound-specific Δ15N analysis of amino acids. Geochim. Cosmochim. Acta **220**: 329–347. doi:10.1016/j.gca.2017.07.036

Yang, J. Y., S. J. Terence, M. D. Kao, X. Yan, and H. L. Lin. 2017. Examining N cycling in the northern South China Sea from N isotopic signals in nitrate and particulate phases. J. Geophys. Res. Biogeo. **122**: 2118–2136. doi:10.1002/2016JG003618

## Acknowledgments

## Conflict of Interest
None declared.